Applied Energy 343 (2023) 121211

Contents lists available at ScienceDirect

Applied Energy

journal homepage: www.elsevier.com/locate/apenergy

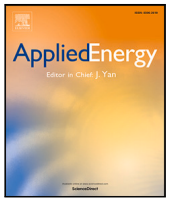

Investigation of hybrid power plant configurations for an offshore vessel with co-simulation approach

Kamyar Maleki Bagherabadi [a,*], Stian Skjong [b], Jogchum Bruinsma [c], Eilif Pedersen [a]

[a] Department of Marine Technology, Norwegian University of Science and Technology, Norway
[b] SINTEF Ocean, Ålesund, Norway
[c] Nedstack Fuel Cell Technology BV, The Netherlands

ARTICLE INFO

Keywords:
Hybrid power plant
Co-simulation
Bond graph modeling approach
System modeling

ABSTRACT

This work presents a full-system simulator consisting of a generic power system integrated with a vessel model and real-time capabilities. The whole system simulation facilitates evaluating the overall system performance by considering components' interactions according to the maneuvering and environmental effects. Indeed, flexibility in the configuration and size of the power system enables the investigation of different concepts according to various maneuvering scenarios. Co-simulation approach is employed to integrate the models with various domains effectively. In addition, the bond graph modeling strategy as a power based method is used. The developed power system contains a diesel genset, a PEMFC, a battery with average electrical components, and a power management system. The configuration of the power system and size of power sources are modifiable. Various hybrid configurations and power capacities can be designed with validated power sources against marine vendors. In addition, the integrated offshore supply vessel with Dynamic Positioning (DP) and cruise controller and sea state forces induces the corresponding load demand of the operation to the power system. In summary, different operation scenarios with sea states, the thrusters' states and allocation algorithm, DC link voltage, power electrical converters controller, and fuel consummations are captured in one model framework. To demonstrate the application of the model and emphasis the importance of total system simulation, three power system configurations are designed and simulated with two operational modes of DP and cruise with various sea states.

1. Introduction

To comply with the strict environmental rules and the energy crisis, new technologies and concepts are proposed to reduce emissions, besides considering the economic and performance [1]. These efforts in the research and industries in the marine sector are conducted through thorough studies of innovative solutions such as alternative fuels, hybridization with Energy Storage Devices (ESDs), employing fuel cells, optimal operational planning, and energy management strategies through the design process. In the last decades, the design process converted to mathematical iterations from physical prototypes in laboratories [2]. These efforts save up costs, reduce the time consumption on the design process, and facilitate the evaluation of a wide range of cases. However, the design and evaluation of multidisciplinary systems such as vessel power plants can be facilitated with ship-wide simulation, which encompasses the various physics and components integration since fully integrated simulations of a vessel with system-level fidelity provide a comprehensive understanding of the system's overall efficiency and components' interaction with real-time capabilities. Moreover, simulations have a significant role in evaluating concepts in the early steps of the designing process and reduce the risk and uncertainty of the system in the final stages of design [3]. In addition, numerical models and simulations with various fidelity can be employed for the design process from concept until manufacturing according to the demanded accuracy. However, multidisciplinary is the primary milestone in developing marine simulators because of the interconnection of various models from different domains and physics. Hence, co-simulation is a proper numerical strategy to integrate the high-fidelity models of multi-domains, which has recently attained more attention in the marine sector.

1.1. Offshore supply vessel

Supply vessels have an essential role in the logistics of the offshore oil and gas industry as multitasking ships with different operations

* Corresponding author.
E-mail addresses: kamyar.maleki@ntnu.no (K.M. Bagherabadi), stian.skjong@sintef.no (S. Skjong), Jogchum.Bruinsma@nedstack.com (J. Bruinsma), Eilif.Pedersen@ntnu.no (E. Pedersen).

https://doi.org/10.1016/j.apenergy.2023.121211
Received 17 June 2022; Received in revised form 4 April 2023; Accepted 24 April 2023

such as DP, cruising, crane, and lifting. [4]. Alongside other industries, fuel efficiency and emission reduction of coastal logistics are the goals to be achieved. Therefore, the fuel cells have proposed new power system configurations in the concept design stage. For example, an offshore platform supply vessel concept powered with diesel generators and methanol-fed Solid Oxide Fuel Cell (SOFC) is proposed in [5]. Improvement in fuel economy, operational flexibility, and less noise and vibration are advantageous to this conceptual design. Also, Ulstein proposed $SX190$ as the first hydrogen-powered supply vessel, in which the power system configuration consists of diesel generators and Proton Exchange Fuel Cell (PEMFC) [6]. Among the solutions for marine power systems and fuel cells, PEMFC has attracted more attention because of proper power density, fast dynamic responses, less noise, and vibration. However, the capital, operational cost, and lifetime are still issues to be solved.

1.2. Hybridization of power plants

Hybridization of power plants with ESDs reduces fuel consumption by allowing the operation of primary power sources close to the optimal region. It improves the dynamic performance of conventional power systems by peak shaving and load leveling. Indeed, ESD as a spinning reserve enhances the system efficiency and reliability [7,8]. Some studies present the hybridization of the power plants with different configurations and study with a system-level model or based on efficiency and load profile statistics. Zhu et al. [9] presented an optimal tug supply vessel power plant design by considering the operating load profile of real recorded operations data. The demanded load power profile is divided into a cruise and an operational service mode. The cruise mode has the most speed and highest power demand. The hybrid topology of the marine power system with good high-level control load sharing can improve fuel efficiency and emission reduction by 10.35 % [10]. Peralta et al. [11] studied the effect of integrating a Li-ion battery into the power system of a platform supply vessel. They have considered and analyzed the system performance in different operations with power statistics demanded to obtain emission reduction improvements. According to the conclusion, a configuration consisting of the main engine, an auxiliary engine, and a battery can reduce the CO_2 emission up to 8.7 %. Lindstad et al. [12] concluded that integration of batteries with conventional engines in offshore supply vessels reduces the emission from 20 % up to 45 %, which depends on location and operational condition. In addition, Jeong et al. [13] investigated the vessel performance with various power plant configurations of conventional propulsion, diesel-electric, and hybrid diesel-electric. It is concluded that hybrid diesel-electric can decrease the annual operational cost of a passenger ferry from 2 % up to 7 % compared with the diesel electrical and conventional propulsion system.

1.3. Modeling of power plants

Pedersen et al. [14] developed a model library for the all-electric marine power plants with the bond graph approach and AC grid with diesel engines and solid oxide fuel cells. The library is developed in a generic configuration to design case studies or retrofit existing vessels. Moreover, it consists of a simplified vessel model and a propeller, which enable investigation of the total system components' interaction with dominated causality. The bond graph modeling strategy is employed for this work. Zahedi et al. [15] presented a DC based hybrid power system with diesel generators and a battery. In addition, a comparison is conducted between average-based assumptions and frequency-based electrical converters. The conclusion depicted a good agreement between the assumptions, besides a significant reduction of computational effort with average-based assumptions. Therefore, in system-wide studies and modeling, the average-based assumption can be employed with reasonable accuracy, which facilities the real-time capabilities of the simulation. Skjong et al. [16] proposed a simulator framework for marine power plants with real-time capabilities and the bond graph method. In this work, the numerical stability, the modeling approach, and controller strategies are emphasized, besides the generic framework of the model. Ghimire et al. [8] developed DC hybrid power system with physical modeling of the electrical components with real-time capabilities. The model can be employed for sophisticated controller design because of considering the switching physics of DC–DC converters. Zhu et al. [17] presented and studied the system-level modeling approach for the DC marine power system by considering the proper physics, which influences the overall system's performances and dynamics. Rokseth et al. [18] presented a model of an offshore supply vessel with rigid body assumption and considered the effect of environmental force and crane interconnection.

There are few works on integrating the power plant and vessel model with unity in fidelity. Bøet al. [19] developed a marine power plant simulator for a semi-submersible drilling rig to study the electrical power availability for various operations and sea states. The simulator consists of a vessel model, thrusters, a mean-value diesel engine model, and generators. The primary contribution was presenting a simulator by considering the interaction of the components to study the power plant dynamics in sophisticated operations. In this work, the Marine Systems Simulator is used as a library of the marine components model with emphasis on the control systems [20]. Skjong et al. [2] demonstrated the application of co-simulation by integrating a vessel model with environmental forces, a power plant consisting of two genset, thrusters, and controllers.

Investigation of the performance of power plant configurations for an OSV to enhance fuel efficiency is a multidisciplinary problem because of special operations such as DP and cruising in various environmental conditions. Regarding the literature review, there is a gap investigation of power plant performance coupled with a vessel model for various operations and sea states. This endeavor requires multi-domain system-level models with real-time capabilities, which can be facilitated with a co-simulation approach.

1.4. Novelty and contribution

This work proposes a system-level modeling approach for a generic hybrid power plant, which captures the power system behavior with various configurations and sizes. The model consists of co-simulation strategy to integrate the high-fidelity model of an offshore supply vessel with environmental forces to the developed power plant. The novelty of this work is an investigation of the power plant configuration of an OSV integrated with a high-fidelity model of the vessel. This integration facilitates evaluating the power plant performance in different maneuvering and environmental conditions instead of one specific load profile. Moreover, the power plant modeling approach and developed high-level controllers provide a generic model in size and configuration, which can be employed to evaluate different configuration concepts with real-time capabilities. The developed model is utilized to investigate the three power system configurations with battery and PEMFCs for an offshore supply vessel. The operation scenarios consist of cruise and DP modes in various sea states to demonstrate the importance of the total system simulation and consider the environmental conditions.

2. Power plant modeling and co-simulation

This section explains the power plant modeling and the vessel model integration by the co-simulation approach. The bond graph approach, as an energy-based mathematical modeling approach, is used. This method is practical for multi-domains systems with various power conversions. The modular view and energy-based approach facilitate capturing various power conversions and power flow through components. This method consists of basic components such as C (storage), I (induction), R (dissipation), TF (transferring), and MTF (Modular transferring). These elements are connected within bonds with a half

arrow, which arrow direction determines the power flow direction. The details of this method and mathematical relations can be found in [21].

This work considers three power system configurations, as shown in Fig. 1. The configuration is designed to investigate the effect of hybridization with one battery the fuel cells on fuel efficiency and power quality. Configuration No. 1, as is shown in Fig. 1(a) has four diesel gensets, which is a typical topology of power system for all electrical vessels. The battery packs are added to Configuration No. 2 as shown in Fig. 1(b) compared with Configuration No. 1. These batteries are considered to investigate the effect of peak shaving and load mitigation on engines. Batteries are employed to reduce the oscillations and slope of the ramp-ups and downs to engines.

Configuration No. 3 is integrated with four PEMFCs fueled by pure hydrogen and a total capacity of 2 MW instead of two diesel engines. This configuration is considered to study the influence of the PEMFC on the emission reduction and low-emission operation modes benchmarked with previous setups. The configuration consists of various power sources with different properties, so a strategy for load sharing is employed. In this work, the load-sharing strategy operates on a rule-based algorithm with wavelet decomposing loads. The concept for the integration of PEMFC with genset for an offshore supply vessel is taken from ULSTEIN SX190 [6] as a zero-emission DP2 construction vessel. The concept of SX190 has a similar power capacity and vessel size to the model of this work. The ULSTEIN SX190 with compressed hydrogen stored in 7×40 ft containers can continue the operation for around four days [22]. The concept of Configuration No. 3 is chosen by the ship design company to ensure feasibility from an installation and operational point of view.

The studies on the power system's performance are conducted in two operations of cruise and dynamics position in various sea states. As mentioned in the literature section, the type of operations and sea states significantly influence the vessel performance and the propulsion system load profile characteristics. The vessel model of an offshore supply vessel developed by [18] is integrated with co-simulation approach. The mathematical model of the components is described in detail in the following sections.

2.1. Power system modeling

The power system consists of electrical and mechanical components and multi-domain power conversions. In this work, the electrical components are modeled based on average-value assumptions [15,17]. This assumption provides enough accurate results for the system-level modeling and significant improvement in the computational time compared with frequency-based models. The mechanical components are modeled based on lumped control volumes and physical relations. The computational effort and the real-time capabilities are essential factors that must be balanced with model fidelity. These assumptions for mechanical and electrical sections reduce the computational effort while providing accurate results of the overall system states. The engine and PEM fuel cell system model are validated against the vendors' products for the marine sector. Hence, the obtained results of the model can estimate the systems' behavior with reasonable accuracy to reality.

2.1.1. Simplified engine model

The diesel engine model is simplified and implemented by the bond graph method as is presented in [14,16]. Indeed, the engine specific fuel consumption and transient response are tuned based on Wartsila 9L20 [23] as is depicted in Fig. 2. This engine is designed for genset application with the power capacity of 1980 kW, in which the minimum specific fuel consumption is achieved on 85 % load and 1680 kW. The dynamic responses of the engine in the figure show 60 s times from idle to full load. However, according to the vendor's specification, idle to full load can be performed in 20 s. This delay has to be considered for shut down the engine in the same manner. In addition, the engine can

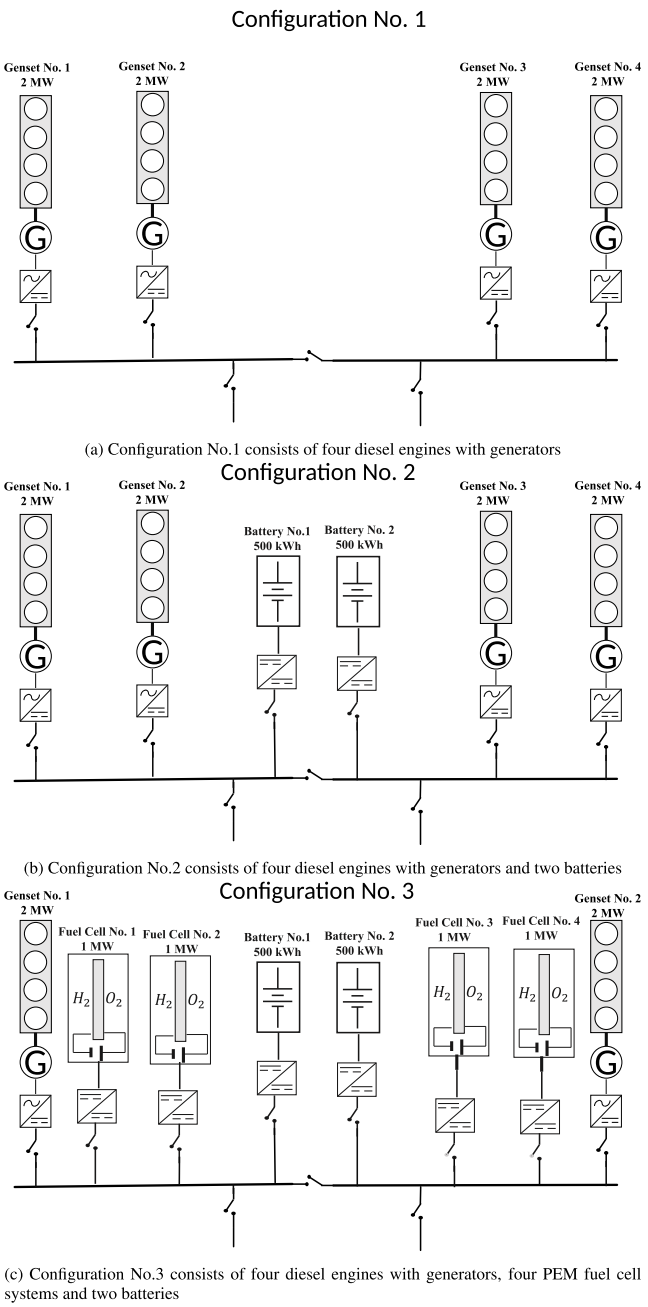

(a) Configuration No.1 consists of four diesel engines with generators

(b) Configuration No.2 consists of four diesel engines with generators and two batteries

(c) Configuration No.3 consists of four diesel engines with generators, four PEM fuel cell systems and two batteries

Fig. 1. The power system configurations with the aim of hybridization.

compensate for the DP operation oscillation loads. The torque by the 4-stroke engine is obtained from Eq. (1) [14]:

$$T_m = \frac{\dot{m}_f}{4\pi b_e(P)} \tag{1}$$

where T_m is the torque, $\dot{m}_f$ is the injected fuel per cycle and $b_e(P)$ is specific fuel consumption as function of engine power.

2.1.2. Synchronous generator

The developed generator from the library of marine power plants with bond graph modeling is used for this model [14]. The model is based on the $(d, q, 0)$ frame, which the detailed relations and explanation can be found here [14,24]. The implemented equations can be written as:

$$U^{SR} = R^{SR} I^{SR} + \frac{d}{dt}\psi^{SR} \tag{2a}$$

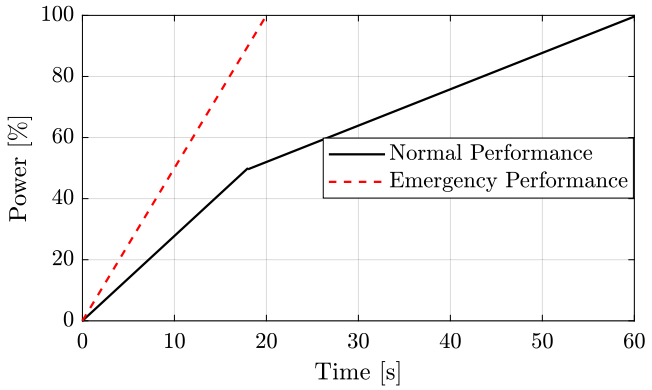

Fig. 2. The engine dynamic performance Wartsila 9L20 [23].

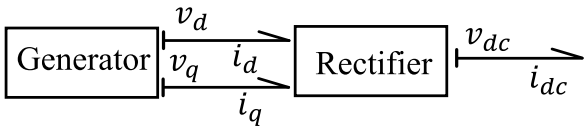

Fig. 3. The bond graph schematic of the rectifier causalities.

$$\psi^{SR} = L^{SR} I^{SR} \tag{2b}$$

$$P = u_d i_d + u_q i_q \tag{2c}$$

$$Q = u_d i_d - u_q i_q \tag{2d}$$

Where U^{SR} is the voltage matrix, I^{SR} is the current matrix, ψ^{SR} is the flux linkage, P is the active power, and Q is the reactive power.

The engine with a proper bond is integrated with the generator to convert the mechanical power to electrical power. The torque is the input to the generator, and rotational speed is the generator output to the engine. The governor controls the rotational speed, which is implemented as a simple PI controller.

2.1.3. Rectifier

The generator is integrated with the DC grid by the passive parametric average value rectifier [25]. The average value assumption for the rectifier provides acceptable results for the DC system [26]. The causality and the bond graph representation of the rectifier are shown in Fig. 3, in which DC grid current and generator voltage are in $(d, q, 0)$ frame outputs. The implemented algebraic relations are given in Eq. (3) [25]. The variable parameters as s function of impedance, which is an accurate implementation for a wide electrical power range.

$$\delta = \arctan\left(\frac{i_d}{i_q}\right) - \phi(z) \tag{3a}$$

$$i_{dc} = \beta(z)\sqrt{i_q^2 + i_d^2} \tag{3b}$$

$$v_q = \alpha(z)\, v_{dc} \cos(\delta) \tag{3c}$$

$$v_d = \alpha(z)\, v_{dc} \sin(\delta) \tag{3d}$$

$$z = \frac{v_{dc}}{\sqrt{i_q^2 + i_d^2}} \tag{3e}$$

where ϕ, β and α are parameters dependent on z as the impedance. The dependency graphs can be found in [25]. i_{dc} is the DC current, v_{dc} is the grid voltage as the input and $i_{d,q}$ is the current on the $(d, q, 0)$ frame.

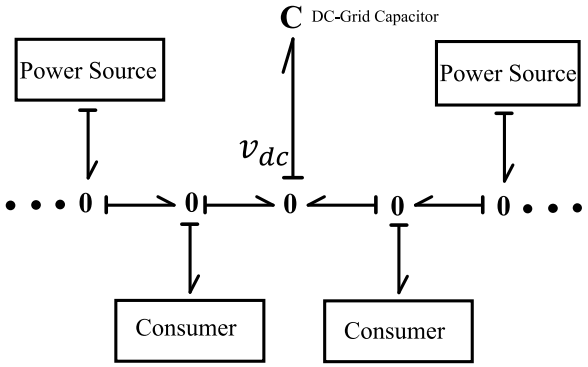

Fig. 4. The bond graph schematic of the DC grid with the bus capacitor, power sources, and consumers.

2.1.4. DC grid

In this work, the DC grid is modeled by a capacitor as the bond graph schematic is depicted in Fig. 4. The mathematical model is based on the well-known Kirchhoff relation in Eq. (4) [27].

The bond graph modular approach facilitates the increasing and decreasing of the number of consumers and sources. This potential allows the generic model to be changed the configuration easily without influencing other components.

$$v_{dc} = \left(i_{sources} - i_{consumers}\right) \tag{4}$$

2.1.5. PEM fuel cell system

The PEM fuel cell system, as is shown in Fig. 5 converts the chemical energy in hydrogen gas directly to the electrical power and water production. The PEM fuel cell system consists of the stack as the heart and auxiliary systems, which provide a suitable condition for the membrane in the cell to transfer the electron and proton. The auxiliary systems are the air supply, the hydrogen supply, the humidifier, and the thermal management. These sub-systems influence the PEMFC system transient responses and the system efficiency significantly [28]. Since hydrogen and oxygen have to be provided at a specific pressure and temperature to the membrane, which consumes power and time. In this model, the air and hydrogen supply systems are considered with constant operational temperature based on the physical relations [29]. The membrane's temperature is assumed constant because its dynamics are at the order of minutes, and the cooling system can maintain the desired temperature [30]. The same assumption for the temperature in system-level modeling for a PEMFC system is made in Ref. [29]. Employing the PEMFCs in the marine sector is different from the vehicle industry from the point of the power capacity and the load profile characteristics [31]. A generic PEM fuel cell system model is used, which can be verified and tuned with various vendors' specifications. The details of this PEMFC system model for marine application can be found in [32]. In this work, the model is validated against and tuned with the Nedstack PEM fuel cell system for marine applications.

The cell voltage is obtained from Eq. (5a), where v_{Nernst} is the reversible potential, v_{act} is activation voltage, v_{ohm} is the ohmic voltage and v_{con} is the concentration voltage. The cell and stack efficiency is affected by the potential losses. The number of cells in series obtains the fuel cell system voltage, and the number of cells in parallel defines the current of the fuel cell system as driven in Eqs. (5b) and (5c). Where, v_{fc} is the fuel cell voltage, $N_{cell_{Series}}$ is the number of cells in series, I_{fc} is the current of the fuel cell system and $N_{cell_{parallel}}$ is the number of cells in the parallel. The net system power is driven from Eq. (5d), where p_{fc} is the fuel cell system net power and p_{aux} is the consumed power by the auxiliary systems. In this work, only the air supply power consumption is included, which is considerable compared with other sub-systems.

$$v_{cell} = v_{Nernst} - v_{act} - v_{omh} - v_{con} \tag{5a}$$

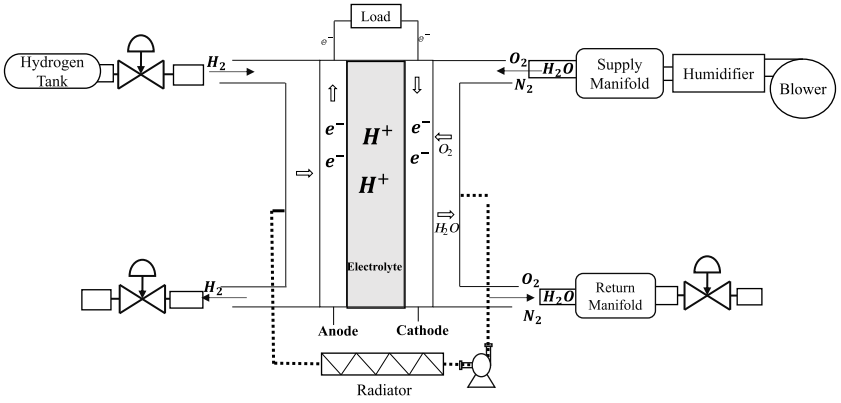

Fig. 5. The schematic of the proton exchange fuel cell system for marine application.

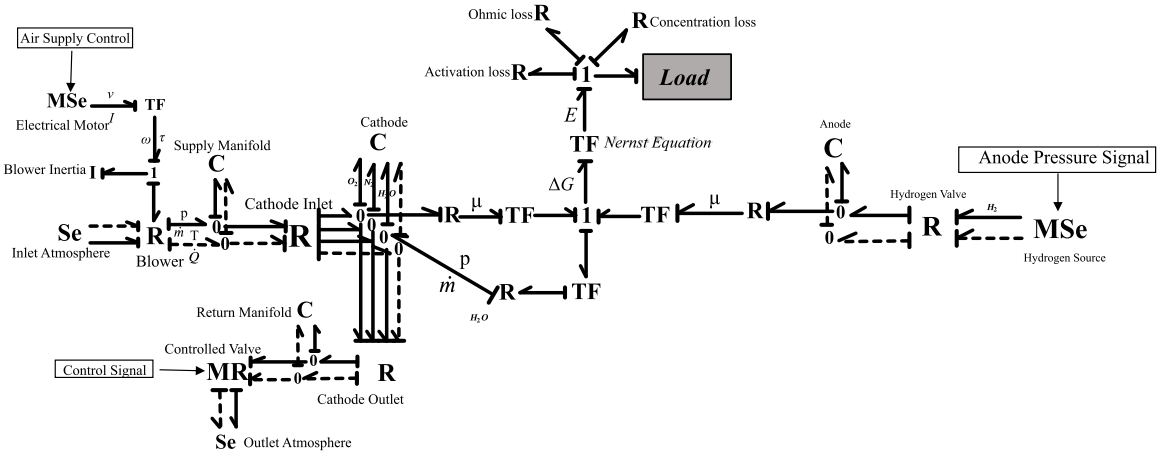

Fig. 6. The bond graph model representation of the PEMFC system.

$$v_{fc} = N_{cell_{Series}} \times v_{cell} \tag{5b}$$

$$I_{fc} = N_{cell_{parallel}} \times I_{cell} \tag{5c}$$

$$p_{fc} = v_{fc} \times I_{fc} - p_{aux} \tag{5d}$$

Fig. 6 shows the bond graph representation of the PEM fuel cell system. The hydrogen supply system is considered ideal because the high-pressure tanks provide it, and it is tuned to the desired pressure by adjusting the inlet valve. However, as depicted in the figure, the air supply system contains the blower and manifolds. The blower inertia, manifold volume, and the outlet control valve determine the system transient responses to the load oscillations and ramps [28].

The static and dynamic behavior of the model is validated against the experimental results of Nedstack marine fuel cells system [33]. The polarization curve validation comparison is depicted in Fig. 7, which has an acceptable agreement with the reference. A slight discrepancy in the low load occurred because of the non-linear behavior of the activation potential loss. However, the fuel cell is not operated in a low load to avoid deteriorating during its lifetime. So, this deviation can be neglected, and the fuel cell is not operated on that load level in this work. The transient behavior is compared with the experimental results shown in Fig. 8. There is good agreement between the model transient behavior and the experimental results. The number of cells defines the fuel cell capacity, which can be chosen according to the demanded power. The PEMFC performance is validated against cell and stack behavior so that the size can be scaled quickly and a good agreement will be achieved. This approach enables producing various power size PEMFCs for power systems [32,34]. To scale the basic model, the number of cells is manipulated, and following the volume of manifolds, the cathode and anode are scaled. The pressure is calculated based on the ideal gas relations, and increasing the volumes affects the dynamics. On another side, the air supplement dynamics by the blower to compensate for the consumed air determined by its inertial affects the voltage dynamics. Hence, by tuning the volumes slightly and blower inertia, the dynamic response of the model approaches in good agreement with the experimental data. Static behavior depends on the cell chemical properties constant in scaling, so the scaling does not affect the static behavior and overvoltages.

Table 1
System specification and operational condition of 1 MW PEM fuel cell system.

Parameter	Description	Value
T_{fc}	Temperature of the stack	65 °C
λ_{O_2}	Stoichiometry of air	2.0
λ_{H_2}	Stoichiometry of hydrogen	1.25
λ	Non-dimensional parameter of the membrane relative humidity	100 %
V_{fc}	The operational voltage range	500 – 1000 V
I_{fc}	The operational current range	0–2400 A
P_{fc}	Power range	1 MW
N_{cells}	Number of cells	120 × 96

The system specifications of the PEMFC and operational conditions are listed in Table 1.

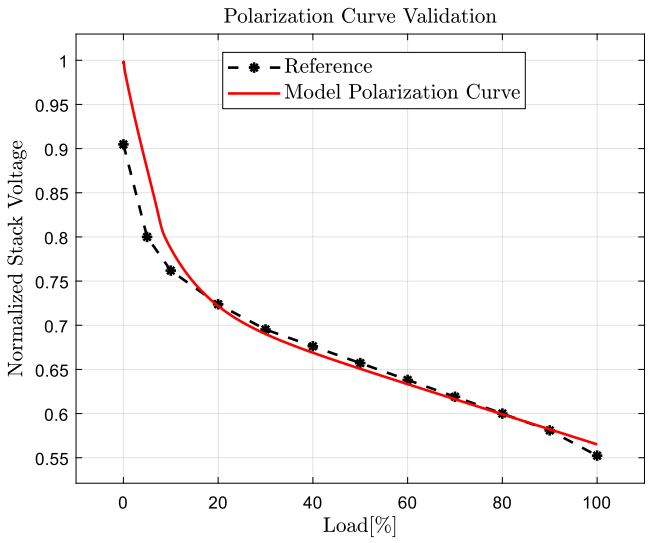

Fig. 7. The validation and tuning of the cell polarization curve.

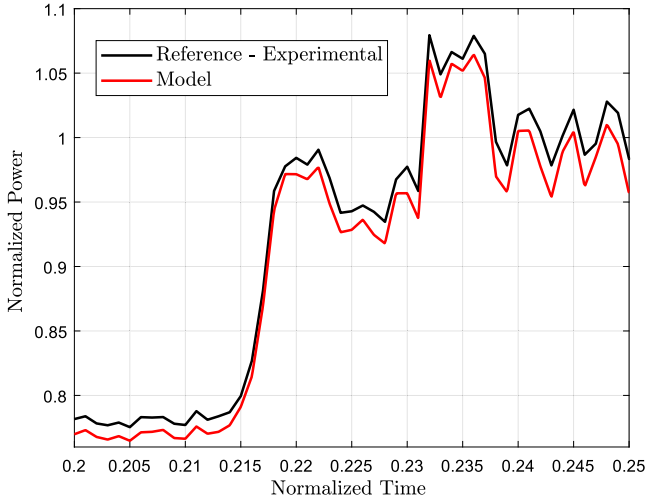

Fig. 8. The validation and verification of the PEMFC system responses.

2.1.6. DC–DC converter-boost

The average-based DC–DC boost converter integrates the fuel cell system into the DC grid. The converters are the low-level controller, which adjusts the output power of the fuel cell by tuning the duty ratio. The duty ratio estimates the switch and diode behavior with continuous operation. The employed controller with duty ratio as the output according to the demanded power for this converter is explained in Section 3.2. The equivalent electrical circuit and the bond graph representation of the model are depicted with average-bases assumptions in Fig. 9 [35]. Therefore, the bond graph method simplifies the high frequency and discrete operation of the switch and diode with a continuous modulated transfer component in bond graph method (MTF) with duty ratio as a variable.

2.1.7. Lithium ion battery model

The equivalent electrical circuit and the bond graph representation of the modeled battery are depicted in Fig. 10. The resistances' coefficients are dependent on the State of Charge (SOC) and the temperature, which is estimated by a fifth-order polynomial curve fitting with experimental results in [36]. The battery pack power is obtained from Eq. (6), in which $V_{battery}$ is the voltage of the battery, $I_{battery}$ is the current of the battery, and N_{cells} is the number of cells. Like fuel cells, the number of cells defines the battery capacity and determines the battery's power capacity. In this work, two battery units are considered with the capacity of 500 kW h and C-rate of 3. C-rate is the battery rate for the charge and discharge.

$$p_{battery} = V_{battery} \times I_{battery} \times N_{cells} \tag{6}$$

The battery SOC indicates the stored energy in the battery, which is obtained from Eq. (7). Where $Q_{battery} = 31$ Ah is the charging capacity of the battery cell. When SOC indicates 1, the battery is fully charged, and indicating 0 means fully discharged.

$$Q_e(t) = \int_o^t I_{battery}(\tau)\, d\tau \tag{7a}$$

$$SOC = 1 - \frac{Q_e}{Q_{battery}} \tag{7b}$$

The dynamics of the battery cell temperature are considered by Eq. (8). Where T_{cell} is the battery cell temperature, $hA = 0.51\,\mathrm{WK}^{-1}$ is the heat convection coefficient with natural convection assumption, $C_T = 2.04 \times 10^6\,\mathrm{jm}^{-3}\mathrm{K}^{-1}$ is the heat capacity of the cell and $T_{air} = 298$ K is the air temperature [36]. In this work, $N_{cells,battery}$ is 5000 with voltage of 700 V and maximum current of 2200 A. The parameters of the equivalent circuit of the modeled battery are given in the Appendix.

$$\frac{dT_{cell}}{dt} = \frac{hA}{C_T}\left(T_{air} - T_{cell}\right) + \frac{1}{C_T} Q_{El,resistance} \tag{8}$$

2.1.8. Bi-directional converter

Since the sign of power flow to the battery changes regarding the charge or discharge state, the buck-boost converter (bi-directional) is implemented. The batteries are integrated into the DC grid by the bi-directional converters with average-based assumption as the electrical circuit. The bond graph representation is shown in Fig. 11 [35]. The duty ratio as the low-level control variable is tuned by a simple PI controller, which is explained in Section 3.2. The values for the power converter and DC link are given in the Appendix [27].

2.1.9. Propulsor and inverter

The propulsion system consists of the propeller, the induction motor, and a PI controller to tune the adjusted torque for the desired thrust. The employed model is used from NTNU marine power system library with the bond graph approach [14]. The asynchronous motors are integrated with the DC bus with an average-based inverter [15]. The relation to obtaining the motor current is expressed in Eq. (9). Where I_{dc} is the DC current as of the consumer from the grid, m is the modulation index, ϕ_2 is the initial phase angle, and ϕ is the d-q transformation angle. These variables are obtained from the controller inside the thruster model.

$$\begin{bmatrix} v_q \\ v_d \end{bmatrix} = \begin{bmatrix} sin(\phi_2 - \phi) \\ cos(\phi_2 - \phi) \end{bmatrix} m V_{dc} \tag{9a}$$

$$I_{dc} = m\left(\left(i_q sin(\phi_2 - \phi)\right) + i_d cos(\phi_2 - \phi)\right) \tag{9b}$$

2.2. Vessel model

The model of an offshore supply vessel presented in [18] with simplified hydrodynamics assumptions is used in this work. The vessel model hydrodynamics is based on the wave potential theory and considers the second-order mean drift forces and consists of a wave filter, DP controller, and cruise controller. In addition, the model contains a thruster model with non-angular MPC thrust allocation to mitigate the load oscillation on the power system [37]. The vessel has three thrusters, two azimuth thrusters at the stern and one fixed thruster at the bow, which produce a force on the sway direction. The main

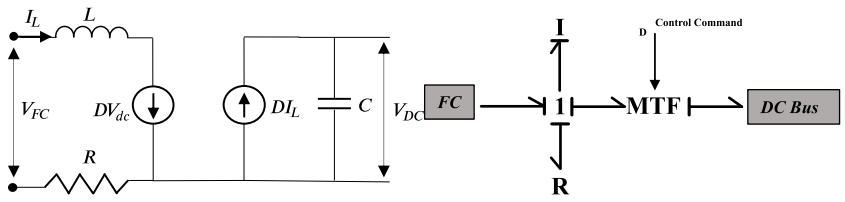

(a) Equivalent electrical circuit representation of the modeled boost converter with the aver-age based assumption (b) The bond graph representation of the mod-eled buck converter

Fig. 9. The electrical circuit and the bond graph representation of boost converter for the fuel cell systems integration to the DC link.

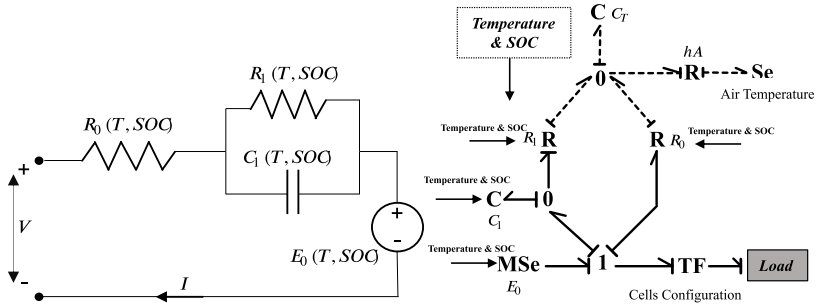

(a) Electrical circuit diagram of the modeled battery [36] (b) The bond graph implementation of the modeled battery

Fig. 10. The battery model.

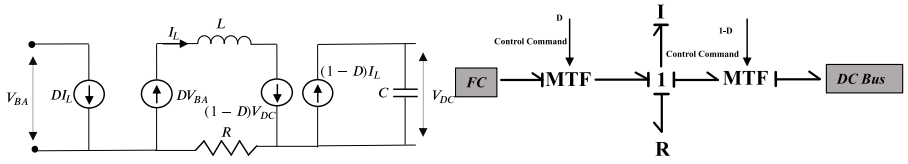

(a) Electrical circuit diagram of the modeled battery [36] (b) The bond graph implementation of the modeled battery

Fig. 11. The equivalent circuit and the bond graph representation of the employed model of the bidirectional DC–DC converter.

vessel parameters are given in Table 2. The trajectory-tracking control in 3 DOF with PID controller is employed in the model to simulate the cruise mode with constant heading and desired surge speed [38]. The bond graph implementation of the vessel model is shown in Fig. 12. The model details are given in [18]. However, some of the primary relations are described in the following. The hydrodynamic damping forces τ_{fv} and torques $\tau_{f\omega}$ are given in Eq. (10) [39].

$$\tau_{fv} = D_{NLv}(v_s) + D_{Lv}v_s$$
$$\tau_{f\omega} = D_{NL\omega}(\omega_s) + D_{L\omega}\omega_s \quad (10)$$

Where v_s and ω_s are the velocity vector for the vessel relative to water velocity, respectively, $D_{NLv}(v_s)$ and $D_{NL\omega(\omega_s)}$ and are nonlinear damping forces and $D_{Lv}v_s$ and $D_{L\omega}\omega_s$ are diagonal matrices of linear friction coefficients.

The exciting forces on the vessel by the wave are calculated by Eq. (11) [39].

$$\Phi = \frac{g\zeta_a}{\omega_W} e^{kz} cos(\omega_W t - kz + \epsilon) \quad (11)$$

Where ζ_a is the wave amplitude from JONSWAP wave spectrum, ω_W is the wave frequency, g is the gravitational acceleration, k is the wave number, z is the vertical distance compared to the surface, t is the time ϵ is a random phase angle [18,39].

The lift force L and drag force by the propeller in the propulsion system are calculated by Eq. (12).

$$L = \frac{1}{2}\rho_w v^2 A C_L sin(2\alpha)$$
$$D = \frac{1}{2}\rho_w v^2 A C_L sin(2\alpha) \quad (12)$$

Where ρ_w is the water density, v is the velocity of the propeller propagating through the water, A is the propeller duct cross-section area, C_L and C_D are the lift and drag coefficients, and α is the angle between the propeller blade and the water velocity [39].

The thrust force T and propeller torque Q are calculated by Eq. (13).

$$T = Lcos(\alpha_p - \alpha) - Dsin(\alpha_p - \alpha)$$
$$Q = 0.7R(Lsin(\alpha_p - \alpha) - Dcos(\alpha_p - \alpha)) \quad (13)$$

Where α_p is the propeller pitch angle and R is the length of the propeller angle [39].

2.3. Co-simulation and models integration

The schematic of the subsystems and connections are illustrated in Fig. 13. The causality between subsystems interconnections is implemented based on the bond graph approach, in which the multiplications of the communicated signal obtain the power flow. As shown in Fig. 13,

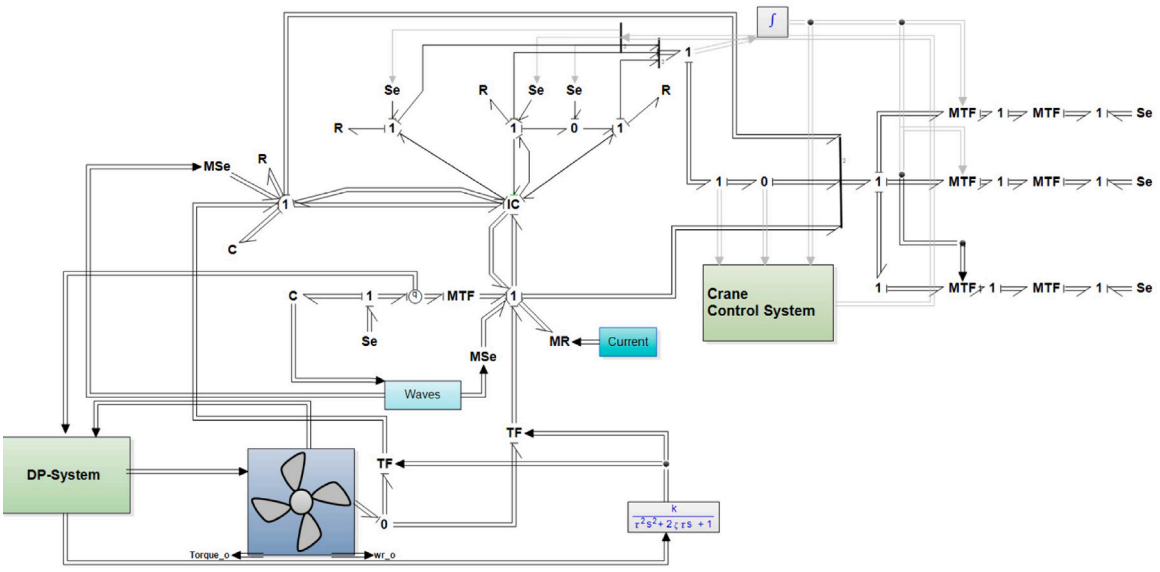

Fig. 12. The bond graph implementation of the vessel model [18,37].

Table 2
The primary parameters of the vessel model and the wave condition [37].

Parameter	Description	Value
L	Length of vessel	107 m
B	width of vessel	22 m
D	Draught of vessel	5 m
H_s	Significant wave height	1 m
T_p	Wave peak period	8 s
N_w	Number of wave components	50
γ	Jonswap-spectrum parameter	1 m
T_d	Lower wave spectra period	0.2 s
T_u	Upper wave spectra period	50 s

the reference subsystem commands the desired position to the controller according to the demanded maneuvering. This is the initiation of the thrust and the power demand. The global thrust is optimally shared between thrusters to mitigate oscillations by an MPC algorithm as a torque set-point to thrusters. Each thruster low-level controller receives the torque set-point according to the demanded thrust. Then the produced thrust is induced in the vessel dynamics, which is simultaneously affected by the thrusters and environmental forces. The obtained position and velocity for the vessel pass the observer as a wave filter to mitigate oscillations and only transfer the low-frequency motions signal to the DP-Cruise controller feedback. The electrical motor provides the requested torque by demanding current from the power system. The power system provides the required electrical power with the constraint of maintaining the voltage constant and the decision of the Power Management System (PMS) on the load-sharing strategy. The PMS as the high-level controller, decided on the load-sharing algorithms based on the load demand signal. Afterward, the demanded power by each component is transferred to its low-level controller.

3. Power management control strategy and low-level controllers

The PMS and the load-sharing strategy for the cruise mode are depicted in Fig. 14. The implemented algorithm in this PMS is rule-based and designed with a generic approach applicable to various configurations. The rule-based PMS is the most common and trustable load-sharing strategy due to its simplicity [9]. The same PMS is used for the three configurations because the logic-statements and the inputs are defined to satisfy the load demand according to other power source states. The employed low-pass filter decomposes the load demands into high and low frequencies. The batteries compensate high-frequency loads and the low frequency with the primary power sources. The priority for the mean power production is by fuel cells to reduce the emission and fuel consumption of the diesel engine as much as possible. Therefore, the fuel cells have more running time compared with the engines. All the primary sources operate on the constant load except Engine No. 1. Genset No. 1 regulates the DC bus voltage. In case of no compensation load by other power sources, this genset provides the demanded load. For example, in Configuration No. 1 which the battery does not exist, the high-frequency load is passively provided by the genset. Therefore, Genset No. 1 operates on part load. In DP mode, high-frequency loads are compensated by batteries for Configuration No. 2 and No. 3, and the mean load in Configuration No. 3 is produced by the first two fuel cells with the same share. In Configuration No. 1 and DP mode, the loads are only compensated with Genset No. 1.

3.1. Load sharing between gensets

There are various control strategies for gensets integrated with other power suppliers in a DC microgrid [40]. In this work, the AVR is used in which the DC grid voltage and the output power of the genset are in Eq. (14). The controller strategy for the gensets is depicted in Fig. 15. The depicted PI controller adjusts the DC grid voltage in Fig. 15. The controller's output is the excitation voltage to the genset and is obtained by Eq. (14).

$$e_v = V_{DC,ref} - V_{DC} \tag{14a}$$

$$e_p = V_{Gen,ref} - V_{Gen_i} \tag{14b}$$

$$V_f = K_{pv} e_v + \frac{K_{pv}}{T_{iv}} \int_0^t e_v \, dt + K_{pp} e_p + \frac{K_{pp}}{T_{ip}} \int_0^t e_p \, dt \tag{14c}$$

Where V_f is the field excitation voltage, K_pv, K_{pp} are the proportional gain of the controller, and K_iv, K_{ip} are the integral time constant of the controller.

3.2. Converters' controller

The boost converter of the fuel cells is controlled by the depicted closed-loop PI controller in Fig. 16. The output of the controller is the duty ratio to the modulated transfer (MTF) as is shown in Fig. 9. The

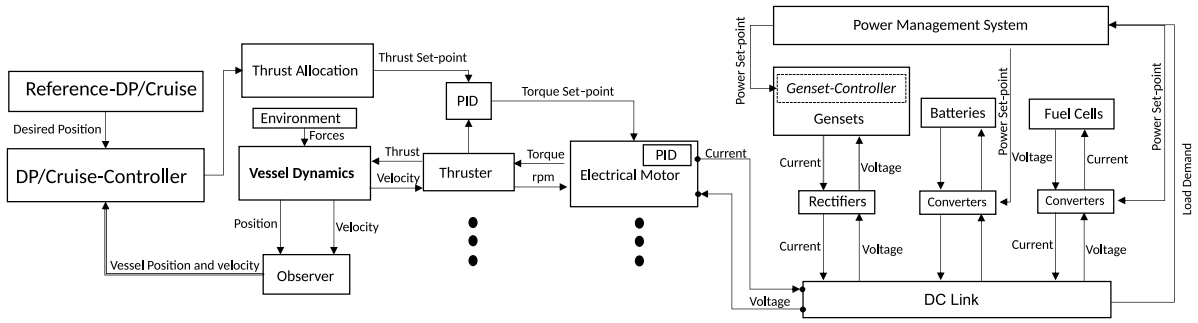

Fig. 13. The schematic of the sub-systems and integration with the causality and the control signals.

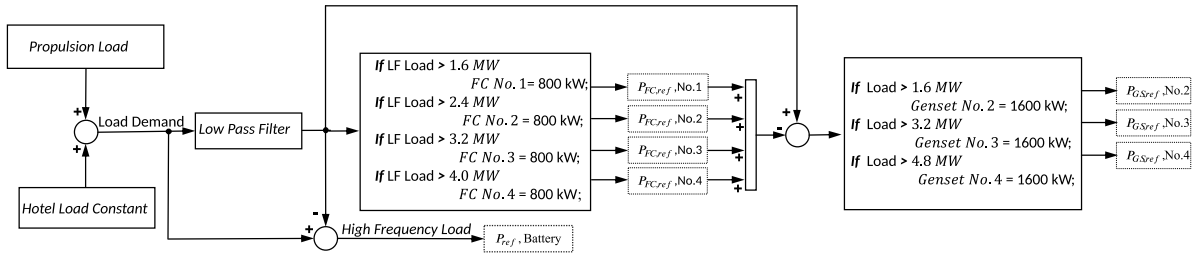

Fig. 14. The power management system strategy in the cruising operation applicable for various power plant configurations.

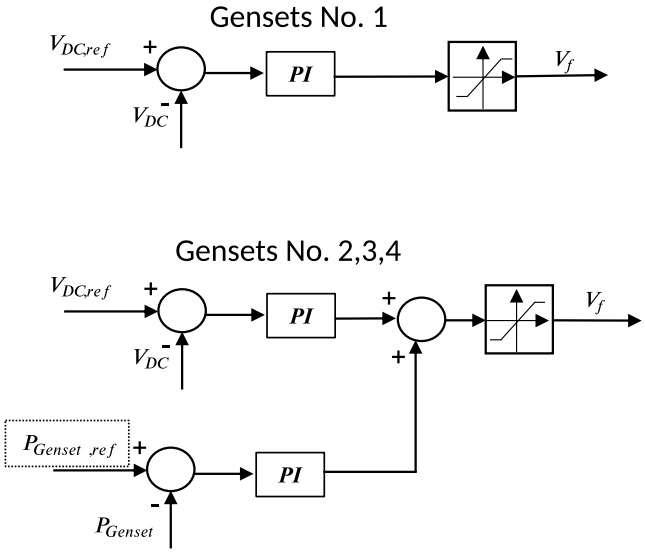

Fig. 15. The genset power sharing controller.

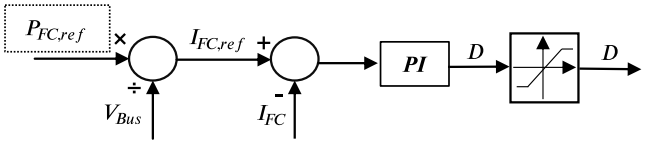

Fig. 16. The boost converter controller.

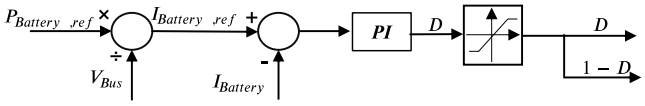

Fig. 17. The bidirectional control strategy.

bi-directional converter controller for the battery is depicted in Fig. 17. The difference compared with the boost converter controller is its two outputs. Since it is designed to operate the battery in the charge and discharge modes, shown in Fig. 11 has two modular transformers. In this work, the battery must compensate for the high-frequency loads, so there are oscillations in the power set-points. The set-point is the power demand from the PMS, which is a constant load in cruise mode, and in DP mode is a part load. The power set-point of the battery comes from the implemented low-pass filter.

4. Simulation set up and designed operations

To study the power plant configurations' performances in various conditions, two operational modes of cruise and DP are designed with a significant wave height of 0, 0.5, and 1 m. The cruise mode requires the highest available power, and the DP mode induces load oscillations. As reported in [4], offshore vessels seldom encounter the calm sea, so it is essential to include environmental forces such as waves in the performance studies. In the cruise mode, the simulation duration is 3600 s, and some steps increase the vessel speed up to 6.5 m/s, then the speed remains constant; afterward, it reduces by step-downs. The set-point cruising speed of 6.5 m/s, which regarding the Ref. [12], is a typical demanded speed for the cruise mode of a supply vessel. The sized power system and the vessel model estimate the behavior of higher speed demands; however, the power system is sized so that the prime movers operate near the optimal region for the demanded power. The significant wave height is considered 0 and 1 m and current from the north direction with a magnitude of 0.1 m/s for this condition to compare the effect of environmental forces on the highest load demand and oscillations. In the DP mode, the simulation duration is 6000 s, and the vessel encounters waves from the north with a significant height of 0.5 and 1 m. The wave properties are given in Table 2. Each power system configuration simulates the designed operational scenarios individually to study the system behaviors and fuel efficiency. The DP scenario is defined as position and heading set-points with station keeping. The hotel and auxiliary load are considered constant 600 kW. The power system configurations and load-sharing strategies are summarized in Table 3. The simulation results are shown and discussed in the following section.

Table 3
The summary of the power system configurations and load sharing strategies.

Config. no.	Power system configuration			Load sharing in DP		Load sharing in cruise	
	Genset	Battery	Fuel cell	Mean load	High frequency	Mean load	High frequency
1	4 × 1980 kW	–	–	GS No. 1	GS No. 1	GS No. 1–4	GS No. 1
2	4 × 1980 kW	2 × 500 kWh	–	GS No. 1	BA	GS No. 1–4	BA
3	2 × 1980 kW	2 × 500 kWh	4 × 1000 kW	FC No. 1, 2	BA	GS No. 1-2, FC No. 1–4	BA

Note: GS = Genset, BA = Battery and FC = Fuel cell.

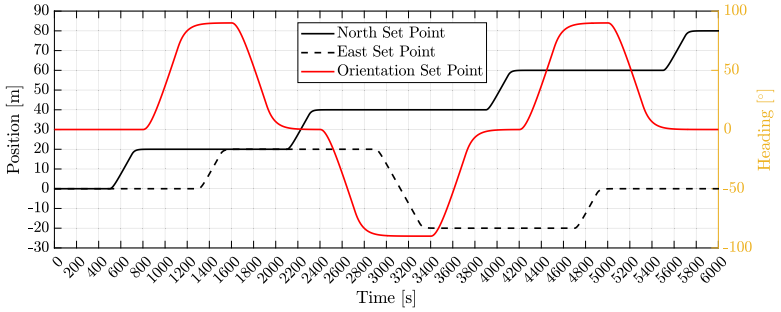

Fig. 18. The reference points to DP controller for heading and orientation. These values passed the damping of the reference model.

5. Results and discussion

This section discusses the results of two operational modes with three power system configurations. The primary purpose is to compare the power system configuration performance from a fuel efficiency and power quality point of view. In the first step, the results of the DP mode operation with a significant wave height of 0.5 and 1 m are presented for three configurations. The results of the three configurations in the cruise mode without wave and a significant wave height of 1 m are discussed in the second step. In addition, the effect of considering environmental disturbances such as waves and currents is demonstrated. As a result, power source behaviors, fuel consumption, controller commands, and vessel positions and speeds are illustrated and discussed.

5.1. Results of DP mode

The set-points from the reference model to the DP controller for heading and orientation in the NED coordinates as the maneuvering scenario are shown in Fig. 18. These values are outputs of the reference model after passing the damping and being smooth. Other set-points are also commanded to the DP controller sequentially. The vessel initiated to move toward the north direction and then 90° rotation to the right. In this orientation, the wave forces encounter the side of the vessel. The operation is finished in the north position of 80 m and the heading angle of 0°.

The vessel position for this operational scenario by the simulation is shown in Fig. 19. The heading is depicted in Fig. 20, which are simulated with two significant wave heights of 0.5 m and 1 m. The wave forces cause disturbance to the vessel position and some discrepancy from the desired position. However, the vessel position converged to the demanded point at the end. The discrepancy from the desired set-point resulted in faster and higher commands of the DP controller to thrusts thrusters to maintain the desired position. The vessel orientation follows the defined set points in good agreement for the two sea states. This scenario for DP operation is repeated with three power system configurations.

The power system load sharing for Configuration No. 2 is shown in Fig. 21, which consists of the battery to imply the hybridization concept. It should be noted that 600 kW of the hotel and auxiliary load is included. As shown, the higher wave height requires more electrical power and induces significant load oscillations in the power

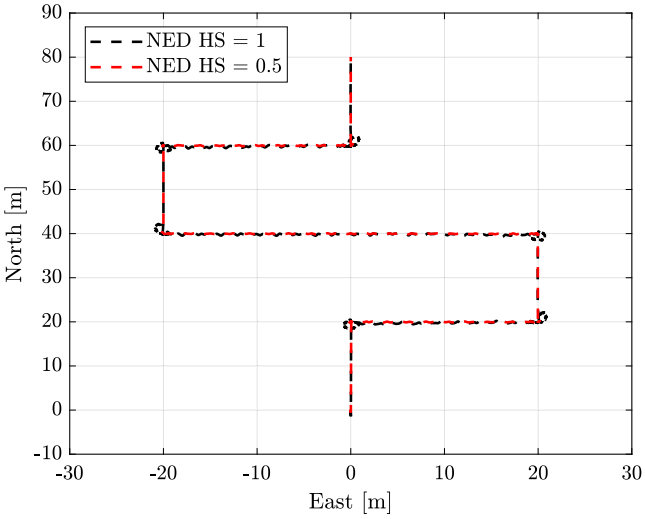

Fig. 19. The vessel position in NED reference with a significant wave height of 0.5 and 1 m.

system. The harsh condition requires more thrust power and faster angle adjustment of the azimuth thrusters, which results in higher mean power and load fluctuations. As is depicted in the figure, the mean load is increased up to 900 kW from 650 kW in a significant wave height of 1 m compared with 0.5 m. The oscillation for the wave height of 0.5 m is not significant; however, for $HS = 1$ m, it is close to 100 kW. In this configuration, the high-frequency load demands are compensated with the battery by the designed low-pass filter. As a result, Genset No. 1 produces the mean load with steady behavior, and load fluctuations are induced in the battery. Three load peaks occurred during this operation; when the vessel moved toward the east and faced the wave forces, and vessel demanded more thrust power to main the position and orientation and, consequently, more burden on the power supplier.

The employed low-pass filter operates correctly because of the steady operation of the engine and induced load oscillation to the battery. Hence, according to environmental conditions, the battery encounters a considerable amount of charge and discharge demands during the DP mode. These oscillations have to be considered to size the battery. In addition, the depth of discharge affects the lifetime of

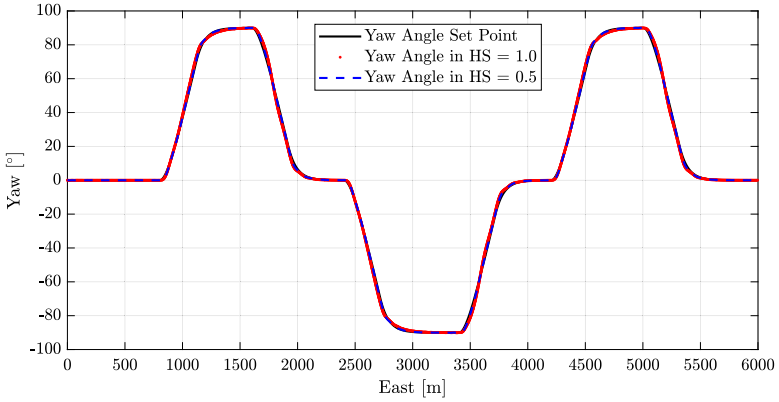

Fig. 20. The yaw angle in DP mode for two significant wave heights.

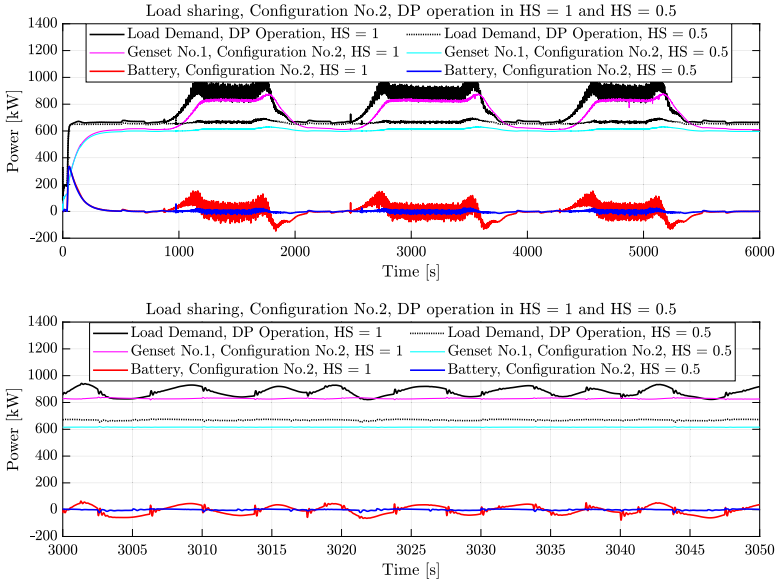

Fig. 21. Comparison of the load sharing in various HS=0.5 m and HS =1 m.

the battery. This indicates the benefits of total system modeling and the importance of considering the environmental effect.

In Fig. 22, the load sharing between power suppliers of Configuration No. 3 is depicted. This configuration consists of fuel cells and batteries and two diesel engines. In this configuration, two fuel cells supply the mean load with the same share. Therefore, Genset No. 1 works low load to maintain the DC link voltage. The battery produces the high-frequency loads of the grid. In the figure, the battery loads of Configuration No. 2 and No. 3 are also compared, which shows the identical value for both. Employing PEM fuel cells and integration with diesel gensets in DP mode resulted in less load demand for the diesel gensets and a reduction of diesel fuel consumption. PEMFCs are capable of supplying part loads as well as constant loads with good efficiency.

In Fig. 23, the comparison of loads on the Genset No. 1 for three configurations in the DP mode is depicted. Employing the battery reduces the load oscillations significantly by comparing the results of Configuration No. 1 and No. 2. The battery conducts the engine to operate on a steady load level with less oscillation. In addition, comparing Genset No. 1 load of Configuration No. 1 and Configuration No. 2 shows the ramp-ups and downs to the engine are mitigated. These ramps are caused by position changing commands to the vessel and moving toward the east. As discussed in Section 3, the engine can supply the ramps in emergency mode and affects the efficiency of the optimal operational region. However, the battery is energy storage and cannot produce power. Therefore, fuel cells in Configuration No. 3 take over the delivery of the mean load and direct the engine to operate in the lowest possible region. By employing fuel cells, this configuration reduces diesel fuel consumption and corresponding emissions.

Fig. 24 compares the DC link voltage for the three configurations. The battery supplies high-frequency loads faster than the Genset No. 1 in Configuration No. 1 without a battery; hence fewer oscillations have resulted in two configurations with the battery. Fuel cells' contribution to the power supply does not significantly affect the bus voltage quality because they produce the mean loads. The high-frequency load and fluctuations, alternating faster than a controller and power source responses, cause dips. There is a slight discrepancy in the obtained voltage from the simulation of configurations No. 2 and No. 3 due to the idle operation of Genset No. 1 to maintain the voltage. In Configuration No. 3, the fuel cell compensates for the mean load, which causes Genset No. 1 to operate in part load. The voltage is maintained at an acceptable tolerance, indicating the stability of the power system and controllers.

The performance and stability of the low-level controllers for gensets and DC–DC converters affect the quality of the DC-grid voltage. As shown in Fig. 25, the field voltage controls the demanded power by the genset and DC converter duty ratio adjust the out power of each fuel cell and battery. The field voltage and duty ratio as control inputs are adjusted to produce the demanded power by the PMS. However, Genset No. 1 has the set-point of the DC-grid voltage and the PMS does not determine the load demand for this genset. In Fig. 25 (top), the duty ratio of the output of the battery converter in Configuration No.

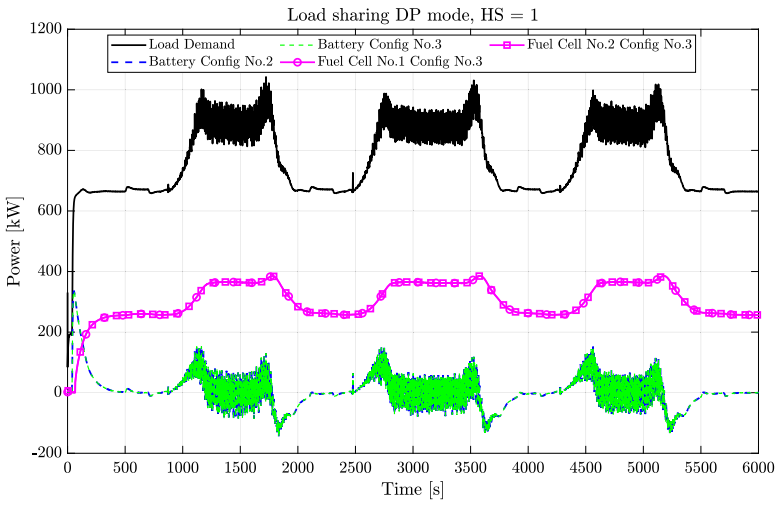

Fig. 22. The load sharing between power sources of Configuration No. 3 and comparison of the battery loads with Configuration No. 2.

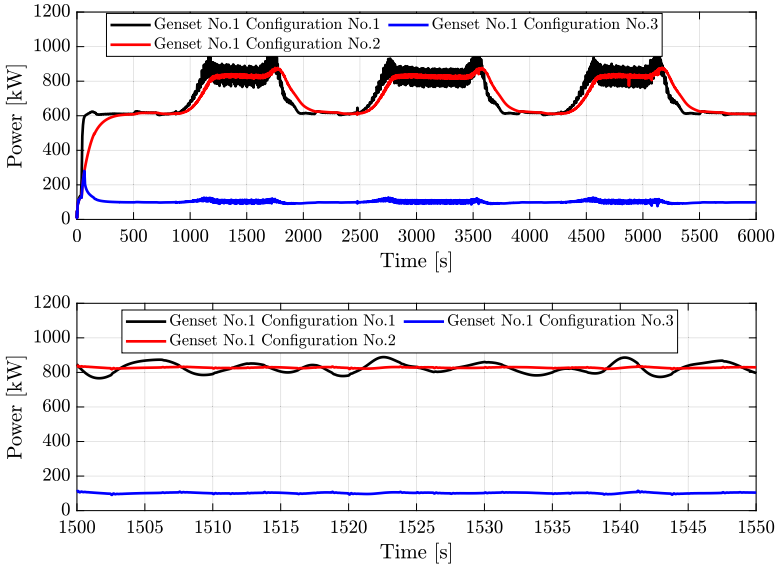

Fig. 23. Comparing the effect of hybridization on Engine No. 1 power production in three configurations for DP mode and significant wave height of 1 m.

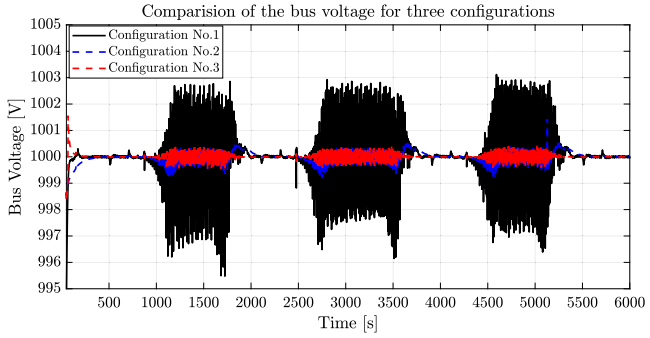

Fig. 24. The voltage of DC link comparison for three configurations in DP mode and significant wave height of 1 m.

3 is depicted, which compensates for the load oscillations and allows the genset field voltage to be maintained steady. The controller output of the field voltage for Genset No. 1 in Configuration No. 1 shows fluctuations since the battery is not employed to handle the oscillations with a faster response.

The comparison between the total amount of fuel consumption by Engine No. 1 for three configurations is shown in Fig. 26. There is a slight difference between employing a battery and without a battery for the engine's fuel efficiency. The load-sharing strategy for the battery is peak shaving, which maintains the engine on the mean load and mitigates the oscillations. This strategy reduces the load fluctuation and not a significant change in the mean load. Also, the specific fuel consumption region does not change, and the fuel consumption is approximately the same. As expected, employing the fuel cells to supply the mean load causes the engine to operate in the idle load. In this case, the total fuel consumption for the defined DP scenario is reduced by 50 %.

5.2. Cruising operation

The vessel's position and surge speed in the cruise mode is depicted in Fig. 27. In this mode, the desired heading angle is fixed on zero, and the speed set-points, as shown in the figure, are increased by steps. The vessel follows commanded speed set-points with a delay due to the inertia of the vessel and the thrusters. The discrepancy in alignment in the vessel position in NED coordinates is induced by the wave forces.

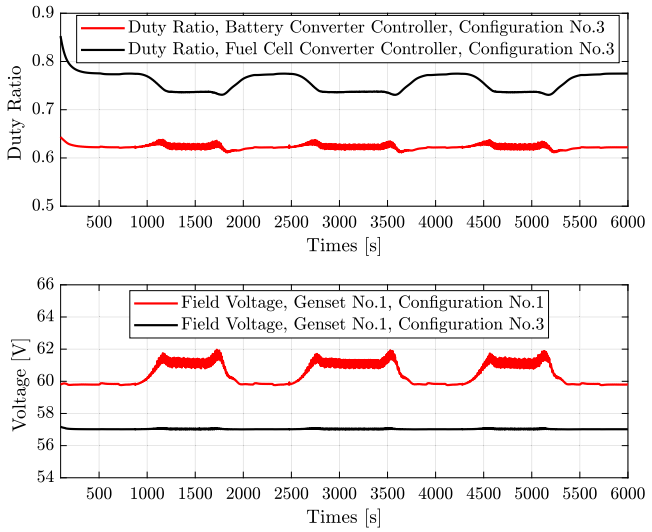

Fig. 25. The voltage of DC link comparison for three configurations in DP mode and significant wave height of 1 m.

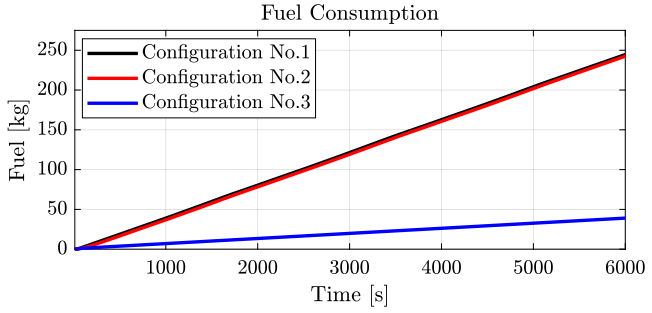

Fig. 26. Comparison of the total amount of diesel fuel consumption with Engine No. 1 during DP operation for three configurations with significant wave height of 1 m.

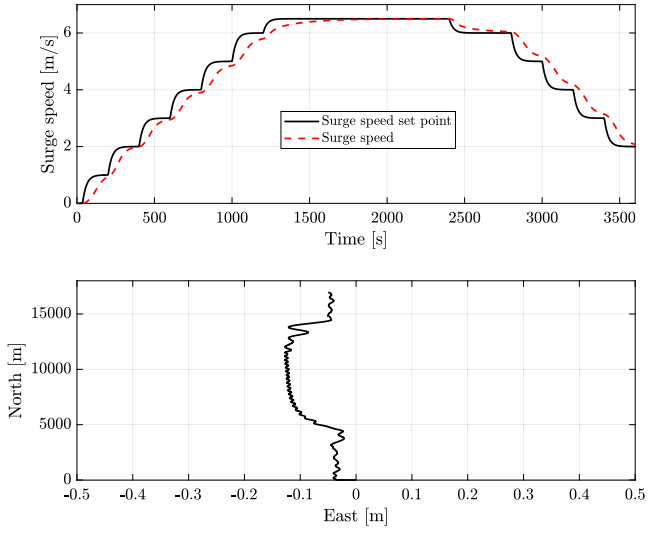

Fig. 27. The position and surge speed of the vessel in cruise mode with the significant wave height of 1 m.

These forces on the vessel are evident at a higher speed when the ship reaches the maximum speed in the middle of the voyage.

The demanded power for this operation is induced to the power system through thrusters, as is shown in Fig. 28. This operation is

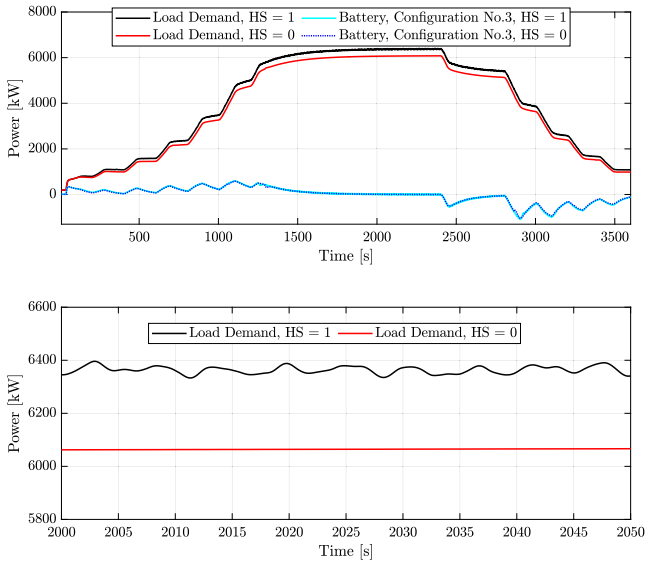

Fig. 28. The load demand and the battery load compensation in the cruise mode in two environmental condition of without wave and with significant wave height of 1 m.

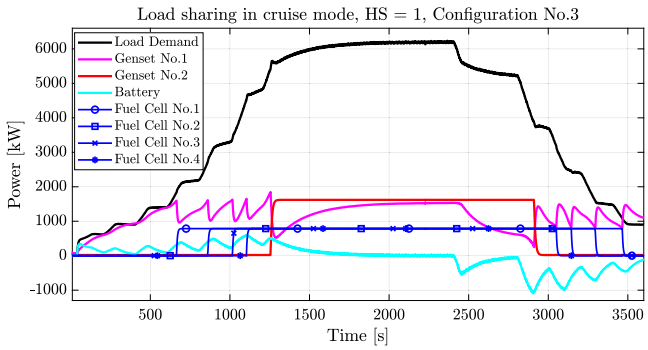

Fig. 29. Load sharing of the power sources in Configuration No. 3 in the cruise mode and significant wave height of 1 m 1*m*.

repeated with two environmental conditions without wave and wave with a significant height of 1 m. The figure illustrates the difference between the load characteristics for the same operation and two environmental conditions. In the maximum surge speed of 6.5 m/s, the difference in power requirements to reach the same speed is increased by about 7 % due to sea states. This is the effect of added mass by the wave. This deviation is increased by increasing the vessel speed. Besides added mass, the waves induce load oscillations in the power system. Sea keeping with the significant wave height of 1 m causes oscillation about 100 kW at the highest speed. The load fluctuations in the cruise mode are less than in DP mode for the same environmental condition. However, in hybrid configurations No. 2 and No. 3, the load oscillations are compensated with the battery, affecting the battery's size and lifetime estimations. In the cruise mode, the start and stop of the power sources, such as fuel cells and gensets influence the battery charge and discharge rate with ramp-ups and downs, as shown in the figure. In this condition, the C-rate of the battery has to be in the range of induced ramp loads.

The load sharing among power suppliers in Configuration No. 3 and cruise mode is shown in Fig. 29. Genset No. 1 takes care of the mean load from the start until the mean load reaches 1.6 MW, then Fuel cell No. 1 starts on the constant load of 800 kW. Four fuel cells start sequentially on the constant load according to the load increment when Engine No. 1 reaches a mean load around 1.6 MW. Each of these start-ups causes a ramp down in Genset No. 1. Meanwhile, the battery

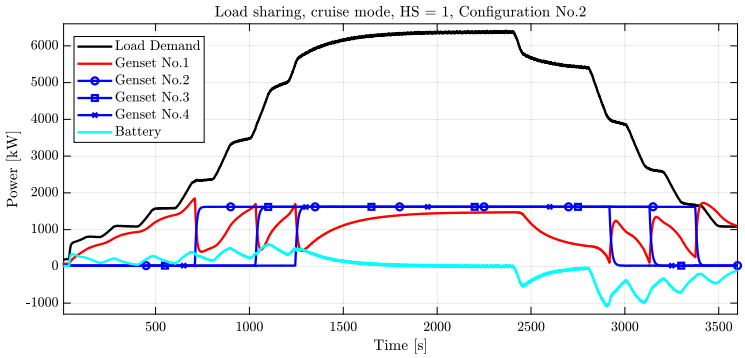

Fig. 30. Load sharing of the power sources in Configuration No. 2 in the cruise mode and significant wave height of 1 m.

compensates for load oscillations and ramps and the demanded power by the engine. Genset No. 2 is the last power source to be turned on and compensate for a portion of the mean load. The fuel cells have the most running time to decrease the diesel fuel consumption by the engines. After the vessel reaches the maximum desired speed of 6.5 m/s, the speed demand and corresponding load decrease. Consequently, the power sources are shut down sequentially. Genset No. 2, as planned by the PMS is stopped first, then other fuel cells are turned off with the same strategy.

In Fig. 30, the load sharing of power sources with the genset and the battery configuration is shown. Compared with Configuration No. 3 is the load supplied by gensets instead of fuel cells. The engine's optimal operational region is around 1.6 MW, so they are turned on to operate on that set-points. This is twice the fuel cells' power capacity; therefore, as shown, the genset starting causes ramp down for Genset No. 1. However, the slope of these ramps is within the safety margin of the engines according to the manufactured product specification [23]. In this case and Configuration No. 1, the engines supply the total demanded load, which consumes diesel as the fuel. The start and stop sequence of the power source in this figure and Fig. 29 illustrates the acceptable performance of the PMS as the high-level controller. The rule-based PMS, as a trustable and straightforward strategy, is widely used in actual cases. This PMS has logic statements and a low-pass filter, which decomposes the load to low and high frequencies. The ramp load and oscillations are induced to the battery, and the low-pass filter's performance is acceptable.

The voltage of the DC-link for the cruise mode for three power system configurations is shown in Fig. 31. As expected, the starting and stopping of the primary power sources cause dips in the DC-link voltage. These oscillations are around 2 % and can be considered in an acceptable tolerance. The battery and fuel cell hybridization weaken these fluctuations in the engines. The battery peak shaving strategy reduces the oscillations by supplying the high frequency faster than Genset No. 1. The voltage maintains its nominal value, which indicates the stability of the low-level power system controllers. As discussed in the previous section, the field voltage and duty ratio of the converter determine the power supply by each power source and, consequently, the DC link voltage.

The battery SOC for Configuration No. 2 in the cruise mode is outlined in Fig. 32. The charge and discharge to the battery are due to compensation of the load steps to mitigate the rate of ramps for the engines. Otherwise, the battery capacity is high enough not to be affected by load oscillations. The oscillation has a harmonic characteristic in the sea keeping; therefore, in the constant speed, the SOC is maintained around 80 % since it operates in approximately the same charge and discharge cycles.

The effect of hybridization by the battery on Engine No. 1 is shown in Fig. 33. The engine without the battery follows load ramps and oscillations, whereas the battery in another topology reduces the engine's rate of steps and fluctuations. The battery load-sharing strategy

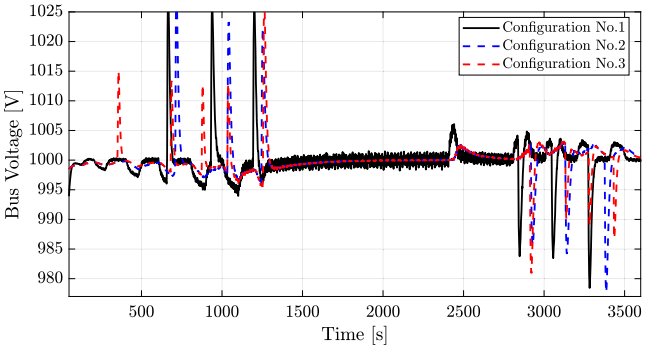

Fig. 31. The voltage of DC link comparison for three configurations in cruise mode and significant wave height of 1 m.

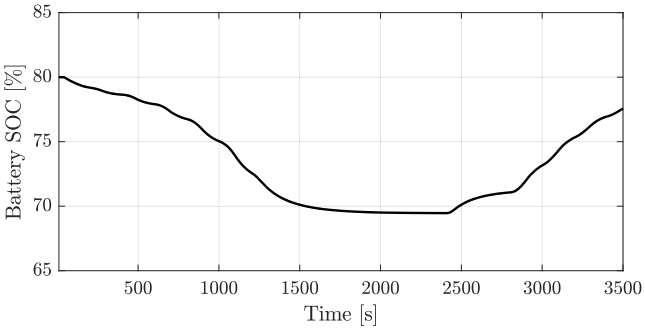

Fig. 32. Battery state of charge for power system Configuration No. 2 in the cruise mode and significant wave height of 1 m.

is based on peak shaving, compensating for the load's high-frequency load characteristics. Therefore, the mean load on the engines in the two configurations is similar and does not change the engines' fuel efficiency in the system-level modeling. However, reducing the oscillation of the engine load improves the lifetime and performance of the engine.

The total fuel consumption during the cruise operation for three configurations is compared in Fig. 34. Integrating the battery with a peak shaving load strategy does not affect fuel efficiency because the battery maintains the engine on the mean load but with fewer oscillations. The load-leveling strategy is an alternative for the battery, which operates the engine on the optimum load and high charge and discharge power rate on the batteries. The battery lifetime is influenced mainly by the depth of discharge. Supplying part of the mean load with hydrogen feed PEMFC decreased the diesel consumption by the engines up to 55 % for this specific cruise operation scenario. It should be noted in Configuration No. 3, 50 % of the total engine power capacity is substituted by the PEMFC.

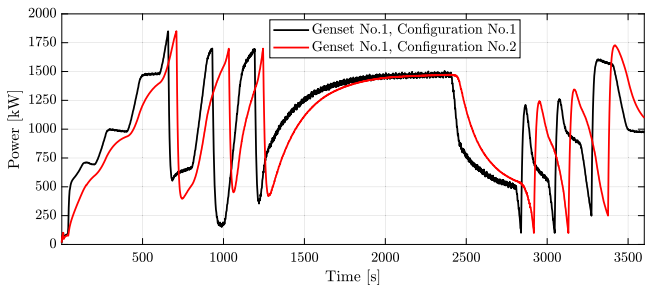

Fig. 33. Comparison of the load on Genset No. 1 by considering the effect of hybridization with the battery.

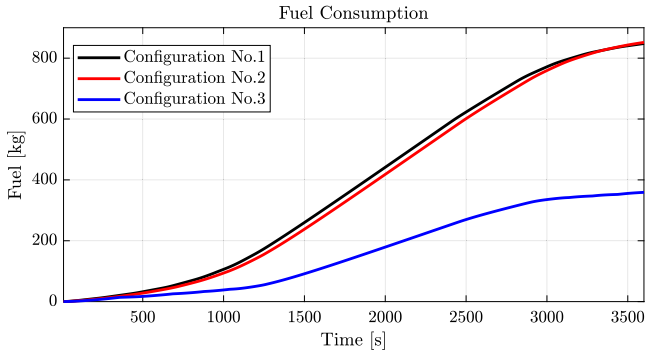

Fig. 34. Comparison of the total amount of diesel fuel consumption with Engine No. 1 in cruise operation for three configurations with a significant wave height of $1m$.

6. Conclusion

This paper presents a generic model of the total vessel system to study hybrid power plant performance for an offshore supply vessel. The model is developed with a modular approach and flexibility in size and operations, which facilitates studying various configurations and power source sizes. In addition, the importance of studying power systems' behaviors integrated with the vessel model is discussed. Moreover, the integrated vessel model has high fidelity, which captures the effect of sea states and environmental conditions. In addition, the models are connected in the co-simulation approach to provide a total system simulation with a reasonable computational time to satisfy the real-time capabilities. Also, the high-level controller as the PMS is independent of the power sources' size and configuration. This strategy reduces the model's complexity to study various power system alternatives. Three configurations are studied in two operations with the same PMS and model structure.

To demonstrate the application of this model, an offshore supply vessel model is integrated with three power plant configurations based on the hybridization concept. The OSVs have two principal operations of cruising and DP mode, and both with environmental conditions are simulated for three configurations. The DP mode with a significant wave height of 1 m induces significant load oscillations to the power system compared with a calm sea state. These fluctuations influenced battery charge and discharge rate in configurations No. 2 and No. 3. This indicates the importance of the integrated modeling of the vessel and power system by considering the environmental conditions. Employing the battery mitigates the load fluctuations on Engine No. 1. However, it does not change the fuel efficiency because of the peak shaving strategy. Employing the hydrogen-fed PEMFC as a substitution as half of the power system capacity decreases the diesel fuel consumption in two operation modes by more than 50 %.

In this work, the method and practicality of the generic total system and simulation have been presented and discussed. The proposed modeling approach and connection in co-simulation method provided the ability to produce power system configurations and evaluate each performance with real-time capabilities. This ability facilitates the feasibility studies in the design stage to assess a wide range of topologies. Moreover, the power and energy management algorithms can be implemented and studied from a fuel efficiency and performance point of view. In future work, various engines, fuel cell systems types, and vessel models can be integrated to provide a wide range of cases and alternatives to be studied.

CRediT authorship contribution statement

Kamyar Maleki Bagherabadi: Conceptualization, Methodology, Software, Validation, Writing – original draft. **Stian Skjong:** Methodology, Software, Writing – review & editing. **Jogchum Bruinsma:** Resources, Writing – review & editing. **Eilif Pedersen:** Supervision, Writing – review & editing.

Declaration of competing interest

The authors declare that they have no known competing financial interests or personal relationships that could have appeared to influence the work reported in this paper.

Data availability

The authors do not have permission to share data.

Acknowledgment

This work is funded by The Research Council of Norway, SFI Smart Maritime and assigned project number 237917.

Appendix

DC-Link capacitor, $C_{dc} = 1\,\mathrm{F}$

DC–DC converter, $L = 0.0005\,\mathrm{H}$

Resistance of converter, $R = 98\,\%$ efficiency

The relation and the parameters of the modeled equivalent circuit of the battery by curve fitting are in the following.

$$C_1 = a_0 + a_1 S + a_2 T + a_3 S^2 + a_4 ST + a_5 T^2 + a_6 S^3 + a_7 S^2 T + a_8 S T^2 + a_9 S^4 + a_{10} S^3 T + a_{11} S^2 T^2 + a_{12} S^5 + a_{13} S^4 T + a_{14} S^3 T^2$$

$$R_0 = b_0 + b_1 S + b_2 T + b_3 S^2 + b_4 ST + b_5 T^2 + b_6 S^3 + b_7 S^2 T + b_8 S T^2 + b_9 S^4 + b_{10} S^3 T + b_{11} S^2 T^2 + b_{12} S^5 + b_{13} S^4 T + b_{14} S^3 T^2$$

$$R_1 = c_0 + c_1 S + c_2 T + c_3 S^2 + c_4 ST + c_5 T^2 + c_6 S^3 + c_7 S^2 T + c_8 S T^2 + c_9 S^4 + c_{10} S^3 T + c_{11} S^2 T^2 + c_{12} S^5 + c_{13} S^4 T + c_{14} S^3 T^2$$

$$E_0 = d_0 S^7 + d_1 S^6 + d_2 x^5 + d_3 S^4 + d_4 S^3 + d_5 S^2 + d_6 S + d_7$$

Where S is the battery state of charge, and T is the cell temperature (see Table A.1).

Table A.1
Parameters of the battery equivalent circuit.

Parameter	Value	Parameter	Value
a_0	−0.06667	b_0	0.01314
a_1	10.78	b_1	−0.0009945
a_2	0.05	b_2	−0.0003607
a_3	−49.68	b_3	0.01936
a_4	1.02	b_4	−6.57e−05
a_5	0.0006667	b_5	6.429e−06
a_6	108.1	b_6	0.09843
a_7	−3.399	b_7	0.0003431

(*continued on next page*)

Table A.1 (*continued*).

Parameter	Value	Parameter	Value
a_8	−0.02006	b_8	2.178e−06
a_9	−100.4	b_9	0.1401
a_{10}	3.521	b_{10}	0.0001028
a_{11}	0.05143	b_{11}	−9.202e−06
a_{12}	31.56	b_{12}	−0.05999
a_{13}	−1.038	b_{13}	−0.0003144
a_{14}	−0.03417	b_{14}	4.929e−06
c_0	0.01515	d_0	24.51
c_1	−0.0546	d_1	−77.94
c_2	−0.0009014	d_2	93.63
c_3	0.09032	d_3	−51.95
c_4	0.003579	d_4	13.31
c_5	1.419e−05	d_5	−1.448
c_6	−0.05373	d_6	0.574
c_7	−0.005509	d_7	3.5
c_8	−5.536e−05		
c_9	0.006349		
c_{10}	0.002883		
c_{11}	8.129e−05		
c_{12}	−4.86e−09		
c_{13}	−0.0001587		
c_{14}	−3.849e−05		

References

[1] Tang R, Li X, Lai J. A novel optimal energy-management strategy for a maritime hybrid energy system based on large-scale global optimization. Appl Energy 2018;228:254–64.

[2] Skjong S, Rindarøy M, Kyllingstad LT, Æsøy V, Pedersen E. Virtual prototyping of maritime systems and operations: applications of distributed co-simulations. J Mar Sci Technol 2018;23(4):835–53.

[3] Sadjina S, Kyllingstad LT, Rindarøy M, Skjong S, Æsøy V, Pedersen E. Distributed co-simulation of maritime systems and operations. J Offshore Mech Arct Eng 2019;141(1).

[4] Aas B, Halskau Sr Ø, Wallace SW. The role of supply vessels in offshore logistics. Marit Econ Logist 2009;11(3):302–25.

[5] Díaz-de Baldasano MC, Mateos FJ, Núñez Rivas LR, Leo TJ. Conceptual design of offshore platform supply vessel based on hybrid diesel generator-fuel cell power plant. Appl Energy 2014;116:91–100.

[6] The ULSTEIN SX190 Zero Emission DP2 construction support vessel. 2022, https://ulstein.com/vessel-design/sx190. [Accessed 22 March 2022].

[7] Miyazaki MR, Sørensen AJ, Vartdal BJJI-P. Hybrid marine power plants model validation with strategic loading, 49 (23). 2016, p. 400–7.

[8] Ghimire P, Zadeh M, Pedersen E, Thorstensen J. Dynamic modeling, simulation, and testing of a marine DC hybrid power system. IEEE Trans Transp Electrif 2020.

[9] Zhu J, Chen L, Wang B, Xia L. Optimal design of a hybrid electric propulsive system for an anchor handling tug supply vessel. Appl Energy 2018;226:423–36.

[10] Geertsma R, Negenborn R, Visser K, Hopman J. Design and control of hybrid power and propulsion systems for smart ships: A review of developments. Appl Energy 2017;194:30–54.

[11] Peralta P CO, Vieira GT, Meunier S, Vale RJ, Salles MB, Carmo BS. Evaluation of the CO2 emissions reduction potential of Li-ion batteries in ship power systems. Energies 2019;12(3):375.

[12] Lindstad HE, Eskeland GS, Rialland A. Batteries in offshore support vessels–Pollution, climate impact and economics. Transp Res Part D Transp Environ 2017;50:409–17.

[13] Jeong B, Oguz E, Wang H, Zhou P. Multi-criteria decision-making for marine propulsion: Hybrid, diesel electric and diesel mechanical systems from cost-environment-risk perspectives. Appl Energy 2018;230:1065–81.

[14] Pedersen TA, Pedersen E. Bond graph modelling of marine power systems. Math Comput Model Dyn Syst 2012;18(2):153–73.

[15] Zahedi B, Norum LE. Modeling and simulation of all-electric ships with low-voltage DC hybrid power systems. IEEE Trans Power Electron 2012;28(10):4525–37.

[16] Skjong S, Pedersen E. A real-time simulator framework for marine power plants with weak power grids. Mechatronics 2017;47:24–36.

[17] Zhu W, Shi J, Abdelwahed S. End-to-end system level modeling and simulation for medium-voltage DC electric ship power systems. Int J Naval Archit Ocean Eng 2018;10(1):37–47.

[18] Rokseth B, Skjong S, Pedersen E. Modeling of generic offshore vessel in crane operations with focus on strong rigid body connections. IEEE J Ocean Eng 2016;42(4):846–68.

[19] Bø TI, Dahl AR, Johansen TA, Mathiesen E, Miyazaki MR, Pedersen E, Skjetne R, Sørensen AJ, Thorat L, Yum KK. Marine vessel and power plant system simulator. IEEE Access 2015;3:2065–79.

[20] Perez T, Smogeli O, Fossen T, Sorensen A. An overview of the marine systems simulator (MSS): A simulink toolbox for marine control systems. Model Identif Control 2006;27(4):259–75.

[21] Karnopp DC, Margolis DL, Rosenberg RC. System Dynamics: Modeling, Simulation, and Control of Mechatronic Systems. John Wiley & Sons; 2012.

[22] The ULSTEIN SX190 Zero Emission DP2 construction support vessel. 2023, https://ulstein.com/news/roadmap-to-a-hydrogen-future. [Accessed 16 February 2023].

[23] The Wartsila diesel genset engines. 2022, https://www.wartsila.com/marine/products/engines-and-generating-sets/generating-sets/wartsila-gensets. [Accessed 29 March 2022].

[24] Tom Arne P. Bond graph modeling of marine power systems. 2009, Faculty of Engineering Science and Technology Department of Marine Technology Norwegian University of Science and Technology.

[25] Jatskevich J, Pekarek SD, Davoudi A. Parametric average-value model of synchronous machine-rectifier systems. IEEE Trans Energy Convers 2006;21(1):9–18.

[26] Zahedi B. Shipboard DC hybrid power systems: Modeling, efficiency analysis and stability control. 2014.

[27] Haseltalab A, van Biert L, Sapra H, Mestemaker B, Negenborn RR. Component sizing and energy management for SOFC-based ship power systems. Energy Convers Manage 2021;245:114625.

[28] Pukrushpan JT, Peng H, Stefanopoulou AG. Control-oriented modeling and analysis for automotive fuel cell systems. J. Dyn. Sys., Meas., Control 2004;126(1):14–25.

[29] Pukrushpan JT, Stefanopoulou AG, Peng H. Control of fuel cell power systems: principles, modeling, analysis and feedback design. Springer Science & Business Media; 2004.

[30] Vasu G, Tangirala A. Control-orientated thermal model for proton-exchange membrane fuel cell systems. J Power Sources 2008;183(1):98–108.

[31] Mo O, Guidi G. Design of minimum fuel consumption energy management strategy for hybrid marine vessels with multiple diesel engine generators and energy storage. In: 2018 IEEE Transportation electrification conference and expo. ITEC, IEEE; p. 537–44.

[32] Bagherabadi KM, Skjong S, Pedersen E. Dynamic modelling of PEM fuel cell system for simulation and sizing of marine power systems. Int J Hydrogen Energy 2022.

[33] 500 kW ned stack fuel cell. 2022, https://nedstack.com/en/pemgen-solutions/maritime-power-installations/pemgen-mt-fcpi-500. [Accessed 02 December 2022].

[34] Bagherabadi KM, Skjong S, Bruinsma J, Pedersen E. System-level modeling of marine power plant with PEMFC system and battery. Int J Naval Archit Ocean Eng 2022;100487.

[35] Janke W. Small-signal transmittances of DC-DC step-down PWM converter in various operation modes. Archives Electr Eng 2015;64(3):505–29.

[36] Huria T, Ceraolo M, Gazzarri J, Jackey R. High fidelity electrical model with thermal dependence for characterization and simulation of high power lithium battery cells. In: 2012 IEEE International electric vehicle conference. IEEE; p. 1–8.

[37] Skjong S, Pedersen E. Nonangular MPC-based thrust allocation algorithm for marine vessels—a study of optimal thruster commands. IEEE Trans Transp Electrif 2017;3(3):792–807.

[38] Fossen TI. Handbook of marine craft hydrodynamics and motion control. John Wiley & Sons; 2011.

[39] Skjong S, Pedersen E. Co-simulation of a marine offshore vessel in DP-operations including hardware-in-the-loop (HIL). In: International Conference on Offshore Mechanics and Arctic Engineering, vol. 57731. American Society of Mechanical Engineers; p. V07AT06A038.

[40] Meng L, Shafiee Q, Trecate GF, Karimi H, Fulwani D, Lu X, Guerrero JM. Review on control of DC microgrids and multiple microgrid clusters. IEEE J Emerg Sel Top Power Electron 2017;5(3):928–48.